Anisotropy dependence of the *c*-axis phonon dispersion in the high-temperature superconductors

Claus Falter, Michael Klenner, and Georg A. Hoffmann
Institut für Theoretische Physik II-Festkörperphysik, Universität Münster, Wilhelm-Klemm-Strasse 10, 48149 Münster, Germany
(Received 1 December 1997; revised manuscript received 2 March 1998)

A recent calculation for La_2CuO_4 using a realistic electronic band structure based on the local-density approximation (LDA) for the description of the electronic density response has predicted a low-lying plasmon branch along the *c*-axis coupling with the phonons of appropriate symmetry. However, the calculated frequency of the plasmon is still high enough to screen the optical phonons more perfectly as seen in the optical *c*-axis spectra which display the typical features of an ionic insulator, namely optical A_{2u} modes almost unchanged from the insulator upon doping. On the other hand, this means that corresponding A_{2u} discontinuities must show up in the phonon spectrum. However, this is in contrast with the current interpretation of the measured *c*-axis neutron data for a $La_{1.9}Sr_{0.1}CuO_4$ crystal looking as is typical for a three-dimensional anisotropic metal in the adiabatic approximation, very similar to what we obtained in our LDA-based calculation. A possible solution for this ''inconsistency'' between optical and neutron results is presented by investigating systematically the dependence of the phonon dispersion along the *c* axis on the anisotropy of the system. Moreover, calculating the phonon-induced changes of the self-consistent potential an electron feels as a function of anisotropy we find that LDA-based calculations, which underestimate the anisotropy of optimally doped LaCuO, lead to a very strong coupling (and thus to a favorable situation for pairing) in the plasmonlike channel. On the other hand, in a more strongly anisotropic scenario the phononlike modes provide a favorable situation for pairing. [S0163-1829(98)04822-X]

A specific motivation for a theoretical investigation of the variation of the phonon dispersion along the *c* axis in the high-temperature superconductors (HTSC's) with the anisotropy of the system is the apparent inconsistency of the (current interpretation) neutron *c*-axis data with the infrared *c*-axis spectra in La-Cu-O. As far as optimally doped and underdoped La-Cu-O is concerned the optical *c*-axis spectra display the typical features of an insulator. They are dominated by optical phonons and are almost unchanged from the insulator upon doping, see, e.g., Refs. 1,2. Only in the nonsuperconducting, overdoped probes are there qualitative changes in the reflectance. Here the spectrum is affected by a component resulting from itinerant electron screening, although the highest-frequency phonon is not completely screened. In addition there is a ''metallic'' temperature dependence of the resistivity along the *c* axis for $x>0.25$, i.e., in the overdoped region of $La_{2-x}Sr_xCuO_4$. These properties point to an anisotropic three-dimensional metal in the overdoped regime. However, the anisotropy even in the overdoped probe seems to be stronger than predicted by a recent study based on a realistic local-density approximation (LDA) band structure taken as input for the calculation of the electronic polarizability Π of La-Cu-O.[3] In this localized description of the electronic density response Π is needed in a localized representation. Thus, the electronic band structure was taken from the complete tight-binding representation of the first-principles linear-augmented plane-wave (LAPW) data including La $5d$, Cu $3d$, $4s$, $4p$, and O $2p$ states as given in Ref. 4 leading to a 31-band model (31 BM). This calculation predicts a low-lying plasmon branch along the *c* axis[3] with a dispersion approximate between 22 and 25 THz. However, the frequency is still high enough to screen the optical phonons more perfectly as seen in the optical experiments. Thus, from the results as obtained in Ref. 3 we conclude that at least optimally doped and underdoped La-Cu-O belongs to a more anisotropic scenario than predicted by LDA.

Next we state the current interpretation of the *c*-axis neutron data as obtained in the experiments for a $La_{1.9}Sr_{0.1}CuO_4$ probe.[5] These data seem to contradict the optical *c*-axis results because they predict a phonon dispersion along the $\Lambda \sim(0,0,1)$ direction being typical for a three-dimensional anisotropic metal as calculated in the adiabatic approximation. This may be concluded from the disappearing A_{2u} discontinuities in the spectrum, being accompanied by the appearance of a Λ_1-symmetry branch with a steep dispersion. Exactly these features are found in the calculations using the 31 BM in the adiabatic approximation[3] (static approximation for the electronic polarizability Π) and also in previous calculations using a simpler 11 band model (11 BM) for the CuO plane.[6,7] A possible solution for this ''inconsistency'' between the optical and the neutron *c*-axis data will be provided below in discussing the question how the degree of anisotropy along the *c* axis does reflect in the phonons. Before proceeding with this item a short review of the theory and the model for treating screening, the electron-phonon interaction (EPI) and the lattice dynamics in the HTSC's is presented. More details are given in Refs. 6–8.

In our theoretical model for the electronic density response and the EPI the *local* part is approximated by an *ab initio* rigid-ion model (RIM) taking ion softening into account as calculated from a tight-binding analysis of the LAPW band structure. Moreover, covalence effects are treated approximatively. Such a model then serves as a reference system for the *insulating* phase of the HTSC's. In case of La-Cu-O good overall agreement throughout the Brillouin zone with the experiments has been obtained.[7] For a description of screening in the *metallic* phase (phonon-

induced) electronic charge fluctuations (CF's) more or less localized on the outer electron shells of the ions depending on the spatial extension of the electron orbitals in the particular shells are considered additionally. The latter dominate the long-range, *nonlocal* contribution to the electronic density response and the EPI. Knowledge of the electronic polarizability Π is necessary to calculate this type of charge response.

Now we present some more details of the theory and the model. As mentioned above the calculation of the *local* part of the density response and of the EPI is performed using a proper *ab initio* model of rigid ions of the Gordon-Kim type to account for the important ionic component of bonding in the HTSC's. The total energy E of the crystal as a function of the location $\{\mathbf{R}\}$ of the ions is given by a sum of self-energies E_0 and pair potentials $\phi_{\alpha\beta}$ of the rigid ions i.e.,

$$E(\{\mathbf{R}\})=E_0+\frac{1}{2}{\sum_{\mathbf{b},\beta,\alpha}}'\phi_{\alpha\beta}(|\mathbf{R}^{\mathbf{b}}_{\beta}-\mathbf{R}^{\alpha}|). \tag{1}$$

$\mathbf{b}$ numbers the unit cells in the crystal and α,β are the different sublattices. $\mathbf{R}^{\mathbf{b}}_{\beta}\equiv\mathbf{R}^{\mathbf{b}}+\mathbf{R}^{\beta}$. The prime in the sum indicates that the term $\alpha=\beta$, $\mathbf{b}=\mathbf{0}$ has to be omitted.

The method of Gordon and Kim[9] is used for the calculation of the pair potentials from the ionic densities. The latter are obtained from a modified version of the Herman-Skillman program including (averaged) self-interaction effects.[10] The unstable free oxygen ion is treated with the help of the Watson-sphere approximation.

As discussed in Ref. 7 the partially covalent character of bonding in the HTSC's suggests to apply somewhat decreased ionic charges as compared with the nominal ones. Such an ion-softening effect resulting in effective charges has been obtained from a tight-binding analysis of the LAPW band structure by calculating the orbital occupation numbers of the corresponding (tight-binding) orbitals in question. The long-range Coulomb contribution to the pair potentials in Eq. (1) is separated and treated exactly using the Ewald method and the remaining short-range part $\tilde{\phi}(R)$ is calculated numerically for different distances between the ions. The numerical result is fitted for convenience by a generalized Born-Mayer-type expression. For it we use the following functional form $f(R)$ for each contribution (electron-nuclei, Hartree, kinetic, exchange-correlation) of $\tilde{\phi}$:

$$f(R)=\pm\exp(\alpha+\beta R+\gamma/R). \tag{2}$$

α, β, and γ are fit parameters.

In order to simulate covalence effects besides ion softening in the calculations, the short-range part $\tilde{\phi}(R)$ of the Cu-O_{xy}, La-O_{xy}, and La-O_z interactions are scaled according to the method proposed in Ref. 11,

$$\tilde{\phi}(R)\rightarrow\tilde{\phi}(R-R_0). \tag{3}$$

The values of R_0 are determined in such a way that the interaction energy in Eq. (1) takes its minimum as close as possible to the experimental structure. The result obtained in this way defines the equilibrium structure for the subsequent phonon calculations. In the case of La-Cu-O the calculated structural parameters are very close to the experimental data applying this procedure.[7] From the pair potentials the dynamical matrix of the ionic reference system is set up using the Ewald method for the long-ranged Coulomb part of the pair potentials. Finally, this model is employed for the description of the *insulating* phase of the HTSC's.

A suitable generalization of this reference model for a description of the *metallic* phase of the HTSC's is achieved by introducing additional long-range, *nonlocal* contributions to the electronic density response and the EPI in the form of more or less localized electronic CF's. The CF's are calculated consistently with the ionic model, allowing for variable occupation numbers of the orbitals. Collecting the *local* and *nonlocal* parts of the density response the central quantity for the lattice dynamics and the EPI in linear approximation, i.e., the displacement-induced change of the electronic density $\mathbf{P}^{\mathbf{a}}_{\alpha}(\mathbf{r})$, can be written as a sum of a rigid (local) contribution and a nonlocal one,

$$\mathbf{P}^{\mathbf{a}}_{\alpha}(\mathbf{r})=\left.\frac{\partial\rho(\mathbf{r})}{\partial\mathbf{R}^{\mathbf{a}}_{\alpha}}\right|_0=[\mathbf{P}^{\mathbf{a}}_{\alpha}(\mathbf{r})]_{\mathrm{RIM}}-\sum_{\mathbf{b}\kappa}\rho_{\kappa}(\mathbf{r}-\mathbf{R}^{\mathbf{b}}_{\kappa})\mathbf{X}^{\mathbf{b}\ \mathbf{a}}_{\kappa\ \alpha}. \tag{4}$$

$\rho(\mathbf{r})$ is the electron density at space point $\mathbf{r}$ and the derivative has to be taken at the equilibrium positions of the ions. The $\mathbf{R}^{\mathbf{b}}_{\kappa}$ describe the localization centers of the CF's in the unit cell (which are identical to the ion locations). $[\mathbf{P}^{\mathbf{a}}_{\alpha}(\mathbf{r})]_{\mathrm{RIM}}$ yields the explicit change of the electronic density due to the movement of the rigid ions and approximates the local part of the EPI. The densities $\rho_{\kappa}(\mathbf{r})$ in Eq. (4) are the form factors of the CF's. They decide upon the local shape and degree of localization of the change in density associated with the different CF's being admitted in the particular model, i.e., consistent with the 31 BM La $5d$, Cu $3d$, $4s$, $4p$, and O $2p$ CF's in the present case.

The quantity $\mathbf{X}$ in Eq. (4) comprises the self-consistent reaction of the CF's in response to an ion displacement. In a physical picture the second term in Eq. (4) contains the electronic polarization of the ionic shells (CF's in our model) nonlocally induced by the phonons. The degree of localization of the CF's varies with their type. The La $5d$, Cu $4s$, $4p$, and the O $2p$ states represent in this context the more extended (delocalized) part of the charge response, while the Cu $3d$ states correspond to the localized more correlated part of the electronic structure leading in our calculations to large on-site Coulomb interactions [$\tilde{V}$, see Eq. (5)] in contrast to the other states. $\mathbf{X}$ can be expressed in linear-response theory in a compact matrix notation as

$$\mathbf{X}=\Pi\varepsilon^{-1}\mathbf{B}\quad\text{with}\quad\varepsilon=1+\tilde{V}\Pi. \tag{5}$$

ε denotes the dielectric function and $\mathbf{B}$ describes the interaction between the CF's and the displaced ions. The effective interaction between the electrons $\tilde{V}$ consists of the direct Coulomb part (Hartree) as well as an exchange correlation contribution. $\tilde{V}$ and $\mathbf{B}$ are calculated from the ionic self-energies and the pair potentials, respectively, by allowing for variable occupation of the orbitals. For the exact definition of $\tilde{V}$ and $\mathbf{B}$ in terms of the derivatives of the crystal energy in the pair-potential-approximation with respect to the ion coordinates and charge-fluctuation degrees of freedom, respectively, see, e.g., Ref. 8. The (static) electronic polarizability $\Pi(\mathbf{q},\omega=0)$, relevant for the *adiabatic* approximation of the

phonons in the density-response approach, can be expressed in the tight-binding representation as

$$\Pi_{\kappa\kappa'}(\mathbf{q},\omega=0)=-\frac{2}{N}\sum_{\substack{n,n'\\ \mathbf{k}}}\frac{f_{n'}(\mathbf{k}+\mathbf{q})-f_n(\mathbf{k})}{E_{n'}(\mathbf{k}+\mathbf{q})-E_n(\mathbf{k})}\times[C^*_{\kappa n}(\mathbf{k})C_{\kappa n'}(\mathbf{k}+\mathbf{q})]\times[C^*_{\kappa' n}(\mathbf{k})C_{\kappa' n'}(\mathbf{k}+\mathbf{q})]^*. \tag{6}$$

The f's, E's, and C's are the occupation numbers, the electronic band structure (Kohn-Sham parameters), and the expansion coefficients of the Bloch functions in terms of tight-binding functions. $\mathbf{k}$ and $\mathbf{q}$ are wave vectors from the first Brillouin zone and N is the number of elementary cells in the crystal. The generalization for $\Pi=\Pi(\mathbf{q},\omega)$ needed in the *nonadiabatic* regime, where dynamical screening comes into play, can be achieved by adding $(\hbar\omega+i\eta)$ to the differences of the ''single-particle energies'' in the denominator of the expression for Π in Eq. (6). Using Eq. (5) for the dielectric function and the frequency-dependent version of the polarizability Π according to Eq. (6), the free-plasmon dispersion can be extracted from the condition

$$\det[\varepsilon_{\kappa\kappa'}(\mathbf{q},\omega)]=0. \tag{7}$$

The coupled mode frequencies of the phonons and plasmons along the c axis must be determined self-consistently from the secular equation for the dynamical matrix [see Eq. (13) below] which contains ω implicitly via Π in the quantity $\mathbf{X}$ in Eq. (5).

Further quantities of interest calculated numerically are the CF's $\delta\zeta_\kappa^{\mathbf{q}\sigma}$ generated by the phonon mode $(\mathbf{q}\sigma)$

$$\delta\zeta_\kappa^{\mathbf{q}\sigma}=-\sum_{\alpha i}X^{\kappa\alpha}_{\ i}(\mathbf{q})u_i^\alpha(\mathbf{q}\sigma)e^{i\mathbf{q}\mathbf{R}^\kappa}, \tag{8}$$

where the displacement amplitudes have been normalized as

$$u_i^\alpha(\mathbf{q}\sigma)=\left(\frac{\hbar}{2M_\alpha\omega_\sigma(\mathbf{q})}\right)^{1/2}e_i^\alpha(\mathbf{q}\sigma). \tag{9}$$

$\omega_\sigma(\mathbf{q})$ and $\mathbf{e}^\alpha(\mathbf{q}\sigma)$ are the phonon frequency and corresponding eigenvector for branch σ and wave vector $\mathbf{q}$, respectively. M_α is the mass of an ion of the sublattice type α. $X^{\kappa\alpha}_{\ i}$ is the Fourier transform of $X^{0\mathbf{a}}_{\kappa\alpha\ i}$ and becomes frequency dependent in the nonadiabatic case.

Furthermore, we calculate the self-consistent change of the crystal potential $\delta V_{\rm eff}(\mathbf{q}\sigma,\mathbf{r})$ induced by the mode $\mathbf{q}\sigma$ at the frequency $\omega_\sigma(\mathbf{q})$ and weighted with the density form factor ρ_κ of the CF κ localized at $\mathbf{R}^\kappa$ in the crystal, i.e.,

$$\delta V_\kappa(\mathbf{q}\sigma)=\int dV\rho_\kappa(\mathbf{r}-\mathbf{R}^\kappa)\,\delta V_{\rm eff}(\mathbf{q}\sigma,\mathbf{r}) \tag{10}$$

with

$$\delta V_{\rm eff}(\mathbf{q}\sigma,\mathbf{r})=\sum_{\mathbf{a},\alpha,i}\tilde{V}^{\mathbf{a}}_{\alpha\ i}(\mathbf{r})u^{\mathbf{a}}_{\alpha\ i}(\mathbf{q}\sigma) \tag{11}$$

and

$$\tilde{V}^{\mathbf{a}}_{\alpha\ i}=V^{\mathbf{a}}_{\alpha\ i}+\tilde{v}P^{\mathbf{a}}_{\alpha\ i}. \tag{12}$$

$V^{\mathbf{a}}_{\alpha\ i}$ stands for the (negative) gradient of the bare ion potential, $\tilde{v}$ is the effective electron-electron interaction, $\mathbf{P}^{\mathbf{a}}_\alpha(\mathbf{r})$ was defined in Eq. (4), and $u^{\mathbf{a}}_{\alpha\ i}(\mathbf{q}\sigma)=u_i^\alpha(\mathbf{q}\sigma)\cdot e^{i\mathbf{q}\cdot\mathbf{R}^{\mathbf{a}}_\alpha}$. The dynamical matrix $t(\mathbf{q})$ takes the form

$$t_i^{\ \alpha}{}_j^{\ \beta}(\mathbf{q})=[t_i^{\ \alpha}{}_j^{\ \beta}(\mathbf{q})]_{\rm RIM}-\frac{1}{\sqrt{M_\alpha M_\beta}}\sum_\kappa[B^{\kappa\alpha}_{\ i}(\mathbf{q})]^*X^{\kappa\beta}_{\ j}(\mathbf{q}). \tag{13}$$

$B^{\kappa\alpha}_{\ i}(\mathbf{q})$ is the Fourier transform of $B^{\mathbf{0a}}_{\kappa\alpha\ i}$.

For completeness the phonon-induced change of the electron density in the mode $(\mathbf{q}\sigma)$ is also given and reads as

$$\delta\rho(\mathbf{r},\mathbf{q}\sigma)=\sum_{\mathbf{a},\alpha,i}P^{\mathbf{a}}_{\alpha\ i}(\mathbf{r})u^{\mathbf{a}}_{\alpha\ i}(\mathbf{q}\sigma). \tag{14}$$

In our model this expression can be decomposed into a local rigid-ion part and a nonlocal charge-fluctuation part, i.e.,

$$\delta\rho(\mathbf{r},\mathbf{q}\sigma)=[\,\delta\rho(\mathbf{r},\mathbf{q}\sigma)\,]_{\rm RIM}+\sum_{\mathbf{a},\kappa}\rho_\kappa(\mathbf{r}-\mathbf{R}^{\mathbf{a}}_\kappa)\,\delta\zeta_\kappa^{\mathbf{q}\sigma}e^{i\mathbf{q}\cdot\mathbf{R}^{\mathbf{a}}}. \tag{15}$$

From the studies rested on the 31 BM for Π in Ref. 3 we find, as already noted, for La-Cu-O a low-lying plasmon along the Λ direction (at about 25 THz at the Γ point in the case where the Fermi energy is taken at the van Hove singularity of the band structure, which is roughly a factor 5 lower than the calculated Drude plasma frequency[12]). This plasmon mixes with the phonons of appropriate symmetry. In such a coupled system we obtain a phononlike and a plasmonlike mode, the latter turns out for the given anisotropy of the 31 BM to be the highest mode in the spectrum. Qualitatively similar results already have been predicted on a less quantitative basis with the extended 11 BM (E-11 BM) in Refs. 7, 8. In this calculation we have generalized the two-dimensional 11 BM introducing interlayer couplings in the parameterized form. Such a model will also be used below in order to investigate the phonon dispersion along the c axis in dependence of the degree of anisotropy by choosing appropriate values for the interlayer coupling parameters.

Our studies in Ref. 3 have explicitly demonstrated that the frequency of the plasmon is determined by the dispersion of the electronic band structure at the Fermi surface along the c axis and is of course also a function of the Fermi energy (of doping in a rigid-band model). We find that for higher doping the anisotropy of the system is reduced, phonons and plasmons decouple and the phononlike mode assumes more and more pure (adiabatic) phonon character. The optimally doped region appears as a crossover region between nonadiabatic behavior at lower doping and adiabatic behavior for higher doping. Altogether, from our calculations in the 31 BM, which certainly are representative for a typical electronic band structure based on the local-density approximation (LDA), we get the important message that phonon-plasmon mixing in a small conelike region around the c axis is a realistic scenario for the HTSC's in the case where a LDA band-structure description for the quasiparticles is appropriate to the calculation of the electronic density response. In other words, the LDA can be applied if there is a

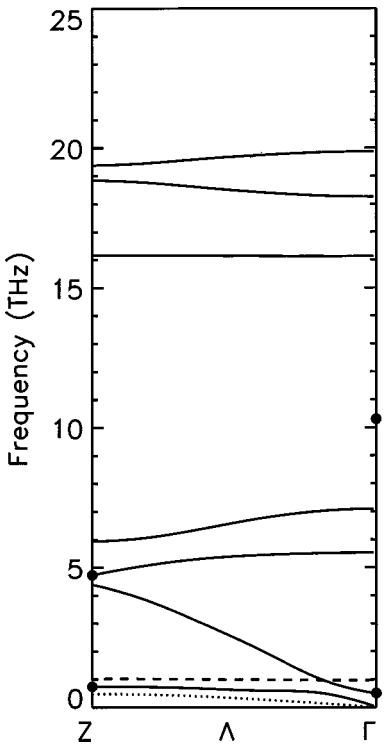

FIG. 1. Calculated nonadiabatic phonon dispersion in the model $M1$ (explained in the text) appropriate for optimally doped La-Cu-O along the $\Lambda\sim(0,0,1)$ direction. — — — — uncoupled plasmon branch; ——coupled phonon-plasmon dispersion of Λ_1 symmetry; · · ·· ·· · · borderline for damping. The lower dot at Z indicates the plasmonlike and the upper dot the phononlike La_z^z mode. The lower dot at Γ indicates the lower of the two coupled LO A_{2u} (ferro) modes (coupled to the plasmon) and the upper dot the TO A_{2u} (ferro) mode. The higher of the two plasmon coupled LO A_{2u} (ferro) modes belongs to the highest Λ_1 branch.

sufficiently large coherent component due to direct hopping of the quasiparticles from wave-function overlap to the charge transport along the c axis. The most likely candidate for such a moderate anisotropic regime is fully oxygenated Y-Ba-Cu-O, but not optimally doped or underdoped La-Cu-O as the optical c-axis results indicate. Here we have an insulatorlike charge response along the c axis pointing to a considerably smaller coherent contribution with increasing anisotropy. Accordingly, we can expect in reality a considerably lower-lying plasmon mode as compared with the LDA-based band-structure calculation of the 31 BM. Moreover, the plasmon should be strongly damped or even overdamped (in particular for its very low frequency), because of the possible coupling of the quasiparticles to the poorly screened nonlocal EPI in the strongly anisotropic case of the HTSC's and the possible correlation effects not contained in the LDA. In the case of a very low-lying plasmon the slowly oscillating electrons cannot screen the long-range Coulomb interactions between the ions and the phononlike mode looks *insulatorlike*, see the results for model $M1$ in Fig. 1 where sufficiently weak interlayer coupling has been assumed. On the other hand, the ions can now follow the oscillations of the electrons and contribute to screening and damping of the plasmonlike mode. However, these damping effects beyond LDA and those introduced by the phonons cannot be calculated within the present model. Optimally doped (and underdoped) La-Cu-O seems to fit this situation quite well in the normal state, i.e., for $T>T_c$.[13,14] Note in this context that on account of the superconducting gap for $T<T_c$ certain EPI effects via low-lying optical phonons may be blocked or not, depending on the size of the gap and damping of the plasmon by EPI may be reduced in the superconducting phase.

It should be added that in the less anisotropic LDA band-structure regime the displacement-induced self-consistent changes of the electron-ion potential δV_κ given in Eq. (10), which are a direct measure for the electron-phonon coupling strength and for pairing, have been calculated in Ref. 3 for the 31 BM and in Refs. 6,7 for the E-11 BM in the case of the apical oxygen breathing mode at the Z point of the Brillouin zone (O_z^z). The interesting result we get, is that for a LDA-like anisotropy the corresponding δV_κ values for Cu d and O_{xy} p orbitals in the *plasmon*like mode are substantially larger than for the phononlike mode and thus provide a very effective channel for pairing with dominating plasmon character.

As far as the efficiency of the phonon-plasmon mechanism for pairing in the strongly anisotropic case is concerned we can say that the plasmonlike δV_κ most likely do not exist because of overdamping. However, the contribution of the *phonon*like δV_κ will be greatly enhanced because of the strongly reduced screening as compared to a system with a large, LDAlike coherent component of the charge transport along the c axis. The δV_κ values at the Cu and the O_{xy} ions in the phononlike O_z^z mode, for example, turn out to be nearly as large as in case of the insulator represented by the RIM, according to our model calculations below. This in turn results in a favorable situation for pairing, this time with a dominating phonon character, however.

In order to classify the HTSC's with respect to their c-axis transport a recently proposed model rested on the Fermi-liquid picture explains the experimental situation quite well.[15,16] Here the out-of-plane charge transport comes from an interplay of the coherent component due to wave-function overlap (direct hopping), impurity-assisted hopping, and phonon- (boson)- assisted interlayer hopping. The relative strength of the coherent and the incoherent contributions varies in the HTSC's depending on the degree of anisotropy from fully oxygenated Y-Ba-Cu-O (strong direct interlayer coupling, nearly coherent), one of the least anisotropic cuprates, to the very anisotropic Bi-based cuprates (very weak interlayer coupling, nearly incoherent). As far as the efficiency of the phonon-plasmon mechanism for pairing in these two extreme cases is concerned we can state that in the first case there is a favorable channel via the plasmonlike modes and in the second via the phononlike modes, see below.

Guided by these findings for the efficiency of pairing in one or the other coupling channel (or eventually in both for an intermediate situation) we could speculate that it should be possible to switch over in a strongly anisotropic material like the Bi-based HTSC's from the phononlike coupling to the plasmonlike coupling by introducing a sufficiently strong covalency in the blocking ionic BiO bilayers, thereby activating the coherent component of the charge transport. Indeed, in a recent experimental study[17] it has been shown that Pb substitution on the Bi site in a single $Bi_2Sr_2CaCu_2O_8$ crystal reduces the anisotropy considerably leading to a de-

crease of the out-of-plane resistivity ρ_c by *four* orders of magnitude. At the same time the temperature behavior changes from semiconductorlike to metallic, without influencing the critical temperature significantly [(Bi,Pb) crystal: $T_c = 82$ K, undoped Bi crystal: $T_c = 87$ K].

Next we study the effect of the anisotropy, in terms of the coherent component of the c-axis charge response, on the phonon dispersion along the Λ direction and on the magnitude of the self-consistent changes of the electron-ion potential δV_κ for selected modes, applying the E-11 BM with several sets of interlayer coupling parameters. In this way the influence of the variation of the bandwidth of the quasiparticles along the c axis, being a direct measure for coherence, can be investigated.

To obtain the results displayed in Fig. 1 a very weak interlayer coupling has been chosen (model $1 \equiv M1$), such that the resulting frequency of the uncoupled plasmon along the Λ direction, as calculated from Eq. (7), is very small. Moreover, the dispersion is very flat. We have about 1 THz in this case (broken curve) which seems to be adequate to simulate the situation of optimally doped La-Cu-O quite well as far as the coherent component is concerned. Also seen in the figure are the *seven* (nonadiabatic) phonon branches of Λ_1 symmetry (full curves) and the borderline for damping due to electron-hole decay (dotted curve).

The plasmonlike branch is further depressed in frequency below the free plasmon and consists of two pieces of different Λ_1 branches characterized by the lower dot at the Γ point and the Z point, respectively. In the (real) optimally doped La-Cu-O crystal this branch seems to be strongly damped or even overdamped for $T > T_c$ as mentioned above.[13,14] The (nonadiabatic) phonon dispersion displayed in the figure looks *insulatorlike* as can be seen by comparison with a study where the nonadiabatic phonon dispersion for the 11 BM has been calculated (model $2 \equiv M2$ in Table I) for the extreme anisotropic limit of a strictly two-dimensional quasiparticle band structure with no coherent contribution along the c axis. In this situation the intraband contribution to the electronic polarizability Π [Eq. (6)] vanishes in a nonadiabatic treatment along the Λ direction (*nonadiabatic insulator*) and the corresponding phonon dispersion in the *metallic* phase is almost indistinguishable from that of the (*adiabatic*) insulator as represented by the RIM, see Fig. 5 in Ref. 7. From these results we deduce the consistency of the measured (insulatorlike) optical c-axis data with the calculated (insulatorlike) phonon dispersion along the Λ direction for the model $M1$ with a small coherent component to the out-of-plane charge transport.

It should be remarked that the RIM from Ref. 7 is used as the reference system for all phonon calculations in the metallic phase presented in this work. As a global covalence effect it takes into account ion softening as calculated from a tight-binding analysis of the LAPW band structure and moreover covalent scaling according to the procedure given by Eq. (3).

As far as the results for the *nonadiabatic insulator* are concerned, qualitatively the same dispersion already has been calculated in Ref. 18, Fig. 5(a), using a less realistic ionic reference system with nominal ionic charges and ignoring covalent scaling. It should be added that in this extreme anisotropic limit the plasmonlike mode along the Λ direction will be soft ($\omega = 0$) and disappears from the spectrum, while the phononlike mode, being the highest Λ_1 mode in the spectrum, is nearly identical to the corresponding uncoupled Λ_1 branch of the ionic insulator (the same holds approximatively true for the strongly anisotropic case displayed in Fig. 1).

TABLE I. Magnitudes of the phonon-induced changes of the self-consistent electron-ion potential δV_κ according to Eq. (10) for the O_z^z and La_z^z mode in units of meV. In the brackets the corresponding frequencies ν in THz are given. The following abbreviations have been used pl: plasmonlike, ph: phononlike, ad: adiabatic, RIM: rigid-ion model. The phonon models $M1-M5$ are explained in the text.

	$\lvert\delta V_\kappa\rvert$, ($\nu$)	Cu	$O_{x,y}$
$M1$	La_z^z(pl) (0.74)	1558.24	1003.90
	La_z^z(ph) (4.73)	148.39	199.73
	O_z^z(ph) (19.38)	587.78	578.78
$M2$	La_z^z(ph) (4.72)	144.62	196.97
	O_z^z(ph) (19.37)	586.42	577.63
$M3$	La_z^z(pl) (3.17)	365.55	178.85
	O_z^z/La_z^z(pl) (5.13)	278.79	294.78
	O_z^z(ph) (19.59)	617.00	603.39
$M4$	La_z^z(ph) (4.17)	41.26	65.67
	O_z^z/La_z^z(pl) (7.97)	803.86	640.80
	O_z^z(ph) (20.48)	742.07	708.72
$M5$	$La_z^z(\approx$ad) (4.24)	22.75	80.95
	O_z^z(ph) (11.99)	429.59	284.29
	O_z^z/La_z^z(pl) (23.77)	1211.35	1104.19
Ad	La_z^z(ad) (4.26)	11.14	84.84
	O_z^z(ad) (15.09)	11.80	79.89
RIM	La_z^z (4.76)	108.24	204.50
	O_z^z (19.38)	606.87	573.46

The dispersion of the c-axis quasiparticle band structure in the models denoted as $M3-M5$ in Table I has been enlarged in such a way that the frequency of the uncoupled plasmon at the Z point takes on values of about 5, 10, and 18 THz, respectively. As a consequence the plasmonlike branch starting in $M1$ below 1 THz is shifted through the spectrum to higher frequencies, increases its width and becomes more and more phononlike. A measure for the width of the coupled phonon-plasmon branch in the different models is provided by the difference in frequency, $\Delta\nu$, of the coupled mode at the Z point and the lower of the two coupled LO A_{2u} (ferro) modes at Γ, respectively. In particular we obtain for $M1$, $\Delta\nu = 0.23$ THz; $M3$, $\Delta\nu = 0.87$ THz; $M4$, $\Delta\nu = 3.36$ THz; and $M5$, $\Delta\nu = 4.95$ THz. The situation for $M1$ and $M5$ is shown in Figs. 1,2. As far as the mode character is concerned, compare with the results of the frequencies for O_z^z and La_z^z as given in Table I.

Owing to phonon-plasmon mixing there exist two longitudinal optical ferroelectriclike A_{2u} modes [A_{2u} (ferro)-LO] at the Γ point (see Figs. 1,2) the lower of which (lower dot) appears below the TO mode (upper dot). The splitting between the lower of the two LO modes and the TO mode decreases as the coherent charge transport along the c axis is more and more activated, see Figs. 1,2 for $M1$ and $M5$, respectively, and finally the A_{2u} discontinuity vanishes in the

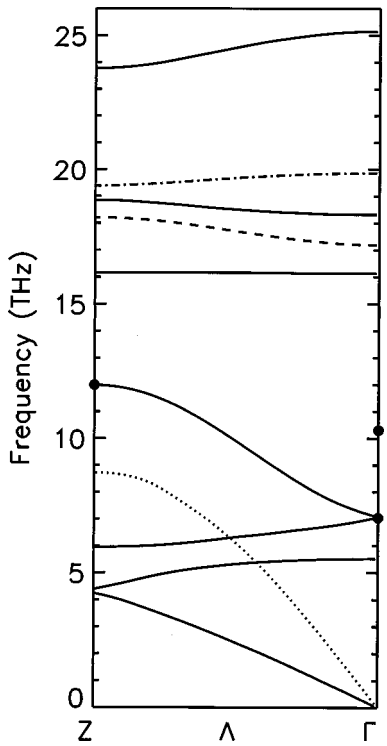

FIG. 2. Nonadiabatic phonon dispersion as calculated in the model $M5$ along the Λ direction. Line types as in Fig. 1. Additionally the uncoupled highest Λ_1 branch of the ionic insulator is shown by the dash-dotted curve. Dot at Z: Phononlike O_z^z mode. Dots at Γ as in Fig. 1.

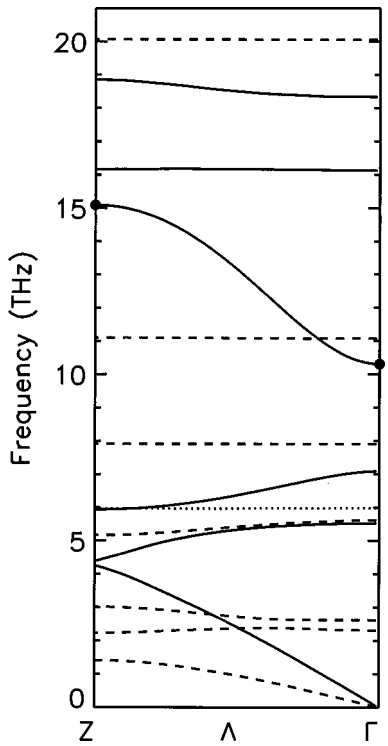

FIG. 3. Phonon dispersion along Λ as calculated for the metallic phase of La-Cu-O in the adiabatic approximation. ——Λ_1- , ····Λ_2- , ---- Λ_3 symmetry branches. Dot at Z indicates O_z^z mode. Dot at Γ indicates A_{2u} (ferro) mode.

adiabatic limit shown in Fig. 3. Simultaneously the typical Λ_1 branch with the steep dispersion ''seen'' in the neutron experiments[5] appears. As a further typical feature of the enlarged interlayer coupling the highest Λ_1 branch in Fig. 2 is moved to higher frequencies away from its uncoupled counterpart (dashed-dotted curve). This Λ_1 branch, which is in the strongly anisotropic regime a phononlike branch, becomes constantly more plasmonlike and ultimately disappears from the spectrum shown, to high frequencies in the adiabatic limit occurring for large interlayer coupling.

In Table I the δV_κ values according to Eq. (10) for the axial oxygen, and the axial lanthanum breathing mode at the Z point, O_z^z and La_z^z, are listed for the models $M1-M5$, the adiabatic metal (Ad) and the (adiabatic) insulator represented by the RIM. Comparing the data for $M1$, which should be representative for optimally doped La-Cu-O with those of the nonadiabatic insulator, ($M2$) and the adiabatic insulator (RIM) we find in all cases for the phononlike modes insulatorlike large values differing not very much. Especially the O_z^z related electron-phonon coupling is very strong and favorable for pairing. Of course the plasmonlike channel via La_z^z in $M1$ would be a very desirable source for pairing, however, this mode seems to be strongly damped or even overdamped in the normal state[13,14] but not in the superconducting phase possibly stabilizing pairing in the condensed phase. Comparing with the adiabatic calculation (Ad) the electron-phonon coupling is strongly increased in the phononlike channel in particular at the Cu ion. It is quite informative from the quantitative point of view that the δV_κ values for the 11 BM in the adiabatic approximation given in Table I are not very far from those of the 31 BM.[3] In the latter case we have for O_z^z at Cu: 16.46 meV and at $O_{x,y}$: 70.12 meV.

The results for the coupling as obtained with $M4$ should be emphasized because here we get two coupled modes of mixed phonon-plasmon character (dominantly O_z^z with a non-negligible La_z^z component in the displacement pattern) leading to large δV_κ's for *both* modes, see Table I. This kind of calculation points to the possibility that the efficiency of the system with respect to pairing can be optimized by tuning the c-axis properties of the HTSC's (e.g., by doping and/or chemical substitution in the ionic layers) in order to give a suitable out-of-plane dispersion for the quasiparticles resulting in an optimal coupling.

With the calculations shown in Fig. 2 ($M5$) we gradually approach the less anisotropic regime. We find significantly larger δV_κ values for the plasmonlike mode as compared to the phononlike one, similarly as for the 31 BM (Ref. 3) and for earlier calculations.[7,8]

A possible solution for the apparent inconsistency of the neutron and optical c-axis data will be presented in the following. In order to investigate this problem we have to calculate the phonon dispersion in a (nonadiabatic) conelike region around the Λ direction with $q_z \gg q_{x,y}$.[3,7,8] Within a very small part of the cone (including the Λ direction) the *charge response is insulatorlike*, provided the c-axis dispersion of the electronic band structure is small enough. While increasing the slope of the wave vector with respect to the Λ direction the charge response becomes more and more adiabatic like in a conventional anisotropic (coherent) metal with a sufficiently high plasma frequency. In our studies we select

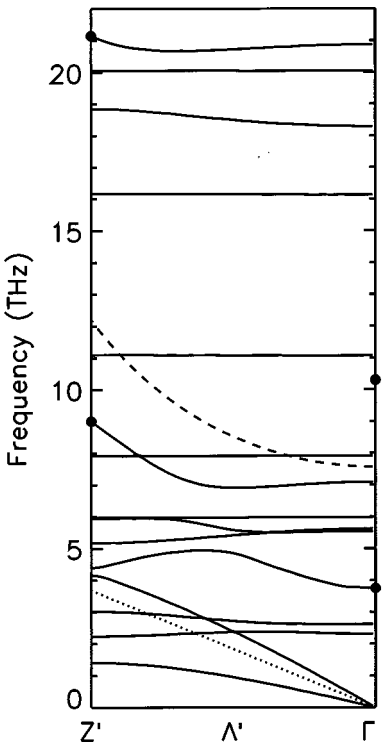

FIG. 4. Nonadiabatic phonon dispersion as calculated with model $M2$ along the Λ' direction defined by $\mathbf{q}=\zeta[\varepsilon(2\pi/a),0,(2\pi/c)]$ for $\varepsilon=0.003$. Only the branches coupling to the charge fluctuations are shown. ——— uncoupled plasmon branch, ···· borderline for damping. Lower and upper dot at Z': Plasmonlike and phononlike O_z^z mode, respectively. Dots at Γ as in Fig. 1.

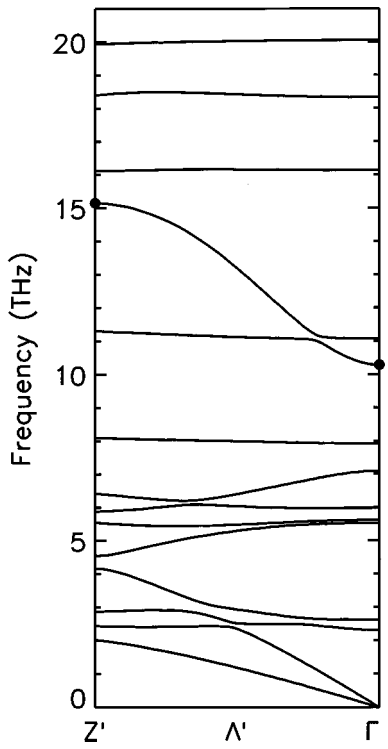

FIG. 5. Same as Fig. 4 with $\varepsilon=0.1$.

for simplicity the extreme anisotropic 11 BM ($M2$) which is practically indistinguishable from the $M1$ model as far as the phononlike branches are concerned. As representative directions in the cone we chose $\mathbf{q}=\zeta(\varepsilon(2\pi/a),0,2\pi/c)$, called Λ' directions, with several values for ε: 0.003, 0.010, 0.025, 0.05, and 0.1. The results for the (nonadiabatic) phonon dispersion in the Λ' directions for $\varepsilon=0.003$ and 0.1 are shown in Figs. 4,5. The symmetry for Λ' is characterized by two irreducible representations (IR's) and only one of these couples to the charge fluctuations. Only phonon branches transforming according to the latter IR are displayed in the figures. Except for the insulatorlike dispersion in Fig. 4 ($\varepsilon=0.003$) the frequency of the uncoupled plasmon (dashed curve in Fig. 4) is too high to be displayed in the presented graphs. The borderline for damping (dotted curve in Fig. 4) is not drawn in Fig. 5. Note that the plasmon frequency rapidly increases with larger ε values because of the quasiparticle dispersion in the (k_x,k_y) plane, see also Refs. 3,8. In Fig. 4 the uncoupled plasmon has about the same frequency as in $M4$. Here we find like for $M4$, two modes with very large δV_κ values (namely the two O_z^z-related modes), indicated by the dots at the Z' point. Different from $M4$ the plasmon has considerably more dispersion which also is reflected in the plasmonlike branch (characterized by the lower dot at Z' and Γ) and the phononlike branch (highest branch in the spectrum). Inspection of Fig. 5 demonstrates that with growing ε values the phonon dispersion approaches the adiabatic result. At $\varepsilon=0.01$ the typical branch with the steep dispersion appears which is found in the adiabatic calculation in Fig. 3. The frequency for O_z^z is already close to the adiabatic result (15.09 THz). However, the ferroelectric split at Γ is still visible. The latter vanishes more and more with larger ε, simultaneously the frequency for O_z^z reaches its adiabatic limit, see Fig. 5. At $\varepsilon=0.025$ we practically enter the adiabatic regime and the dispersion essentially remains unchanged up to $\varepsilon=0.1$.

Now we are in a position to resolve the inconsistency in the optical and the neutron data. Let us assume that in the optical measurements the c-axis polarization can be realized with high precision. Thus we can compare directly with our calculation of the phonon dispersion in the $M1$ model with wave vectors strictly along the Λ direction being insulatorlike (Fig. 1), just as with the optical c-axis spectra. So there is no inconsistency between the calculated nonadiabatic phonon data and the measured optical data in the case where the wave vector is fixed with the same high precision. On the other hand, in the neutron measurements the wave vector cannot be fixed with such a high precision. It seems realistic that the wave vector will scatter inside a conelike region around Λ where the angle at the top of the cone corresponds to an ε value of about $\varepsilon=0.1$. In such a situation the relatively small ''nonadiabatic,'' insulatorlike part of the cone ($\varepsilon<0.003$, see the calculations above) is overbalanced by the significantly larger part where the phonon dispersion is nearly adiabatic ($\varepsilon\geqslant 0.01$). Thus in the neutron experiments essentially the adiabatic, metallic dispersion with vanishing A_{2u} discontinuities and the typical Λ_1 branch (eventually a bit smeared out) with the steep dispersion is ''seen,'' just as our calculation for metallic La-Cu-O in the adiabatic approximation predicts.

Finally, some arguments will be given to explain that increasing ε will lead to the adiabatic regime. In Fig. 6 the

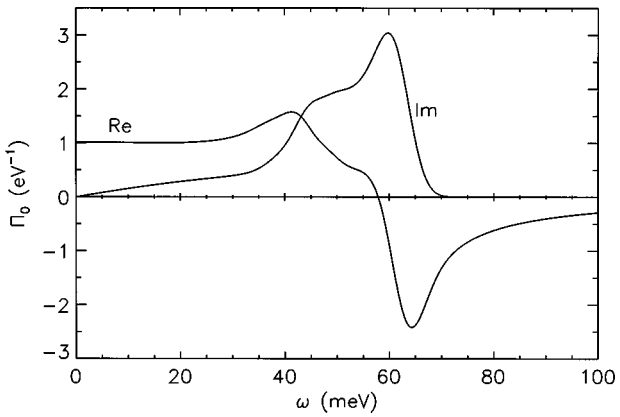

FIG. 6. Frequency dependence of the intraband contribution of the electronic polarizability $\Pi_0(\mathbf{q},\omega)$ at $\mathbf{q}=[0.0125(2\pi/a),0,0]$ as obtained from Eq. (6), taking $C_{\kappa n}(\mathbf{k})=1$ for the eigenvectors. Re means real part of $\Pi_0(\mathbf{q},\omega)$ and Im stands for imaginary part of $\Pi_0(\mathbf{q},\omega)$.

intraband contribution $\Pi_0(\mathbf{q}=[0.0125(2\pi/a),0,0],\omega)$ of the electronic polarizability from Eq. (6) is shown, suppressing the eigenvectors, i.e., taking $C_{\kappa n}(\mathbf{k})=1$. Note that our calculations in Ref. 3 indicate that the characteristic structures as a function of the frequency ω for the (reduced) polarizability Π_0 essentially do agree with the full expression taking into account the eigenvectors, in particular for the dominant (Cu d)-(Cu d) matrix element. The ω dependence of Π_0 scales for small q_x as $\Pi_0(q_x,\omega)=f(\omega/q_x)$. This means that for smaller q_x the characteristic structures of $\Pi_0(\omega)$ are shifted to smaller ω values and for larger q_x, $\Pi_0(\omega)$ is stretched out to larger ω values. Keeping this in mind, we can localize in Fig. 6 the frequency of the O_z^z mode, $\omega(O_z^z)$, for example, for several ε values. For $\varepsilon=0(q_x=0)$ all nonzero frequencies correspond in Fig. 6 to $\omega\rightarrow\infty$ and we have $\Pi_0(\omega)=0$. In this case only the interband contribution to the polarizability remains and we get the nonadiabatic insulator. For $\varepsilon=0.01$ $\omega(O_z^z)$ corresponds in Fig. 6 to $\omega\approx 75$ meV. This frequency is still in the nonadiabatic regime as Fig. 6 indicates and close to the damping region. $\varepsilon=0.025$ (the phonon dispersion looks practically adiabatic) corresponds in Fig. 6 to an O_z^z frequency $\varepsilon\approx 31$ meV. This value is localized in the high-frequency part of the adiabatic regime [passing over to the nonadiabatic region] where $\mathrm{Re}[\Pi_0(\omega)]>0$ and nearly constant while $\mathrm{Im}[\Pi_0(\omega)]$ is small and linear in ω. For larger ε values we stay of course in the adiabatic regime.

Summarizing we have studied the anisotropy dependence of the c-axis phonon dispersion and the efficiency for coupling (pairing) in the phonon-plasmon mechanism in the HTSC's using La-Cu-O as an example. LDA-based calculations underestimate the anisotropy of optimally doped La-Cu-O but lead to a very effective coupling in the *plasmonlike* channel. Fully oxygenated Y-Ba-Cu-O seems to be the most likely candidate for such a scenario. Experimental evidence comes from the results reported in Ref. 19 where the c-axis reflection spectrum of a $YBa_2Cu_3O_7$ single crystal was fitted using phononic oscillators, a midinfrared excitation and a low-energy plasmon. In strongly anisotropic (and extremely anisotropic) materials with a small coherent component to the c-axis charge-transport like optimally doped La-Cu-O (the Bi-based HTSC's) the out-of-plane charge response is (nonadiabatic) insulatorlike and as a consequence the *phononlike* mode provides a favorable situation for pairing. Tuning the c-axis properties by doping and/or chemical substitution in the ionic layers may lead to an optimal coupling scenario. Further we have shown adopting the strongly anisotropic case for optimally doped La-Cu-O that there is no inconsistency between the measured optical c-axis spectra displaying the typical features of an insulator and the calculated *nonadiabatic* phonon dispersion along the Λ direction. Finally, we have proposed a solution for the inconsistency concerning the measured optical data and the current interpretation of the neutron c-axis results by assuming that the wave vector in the neutron experiments cannot be fixed with sufficiently high precision along the Λ direction. In such a situation the relatively small nonadiabatic (insulatorlike) part of the cone around the Λ direction within which the wave vector will be scattered is overbalanced by a significantly larger part where the phonon dispersion looks adiabatic with the typical features due to metallic screening, which already have been predicted by our earlier calculations using the adiabatic approximation for the phonon-induced charge response.

ACKNOWLEDGMENTS

We greatly appreciate the financial support by the Deutsche Forschungsgemeinschaft (DFG).

[1] S. Uchida, T. Ido, H. Tagaki, T. Arima, Y. Tokura, and S. Tajima, Phys. Rev. B **43**, 7942 (1991).

[2] S. Uchida, K. Tamasaku, and S. Tajima, Phys. Rev. B **53**, 14 558 (1996).

[3] C. Falter, M. Klenner, and G. A. Hoffmann (unpublished).

[4] M. J. De Weert, D. A. Papaconstantopoulos, and W. E. Pickett, Phys. Rev. B **39**, 4235 (1989).

[5] L. Pintschovius and W. Reichardt, in *Physical Properties of High Temperature Superconductors IV*, edited by D. M. Ginsberg (World Scientific, Singapore, 1994), pp. 295–374.

[6] C. Falter, M. Klenner, and W. Ludwig, Phys. Rev. B **47**, 5390 (1993).

[7] C. Falter, M. Klenner, and G. A. Hoffmann, Phys. Rev. B **52**, 3702 (1995).

[8] C. Falter and M. Klenner, Phys. Rev. B **50**, 9426 (1994).

[9] R. G. Gordon and Y. S. Kim, J. Chem. Phys. **56**, 3122 (1972).

[10] J. P. Perdew and A. Zunger, Phys. Rev. B **23**, 5048 (1981).

[11] N. L. Allan and W. C. Mackrodt, Philos. Mag. B **69**, 871 (1994).

[12] W. E. Pickett, Rev. Mod. Phys. **61**, 433 (1989).

[13] K. Tamasaku, Y. Nakamura, and S. Uchida, Phys. Rev. Lett. **69**, 1455 (1992).

[14] J. H. Kim, H. S. Somal, M. T. Czyzyk, D. van der Marel, A. Wittlin, A. M. Gerrits, V. H. M. Duijn, N. T. Hien, and A. A.

Menovsky, Physica C **247**, 297 (1995).
[15] R. J. Radtke and K. Levin, Physica C **250**, 282 (1995).
[16] R. J. Radtke, V. N. Kostur, and K. Levin, Phys. Rev. B **53**, R522 (1996).
[17] L. Winkeler, S. Sadewasser, B. Beschoten, H. Frank, F. Nouvertné, and G. Güntherodt, Physica C **265**, 194 (1996).
[18] C. Falter, M. Klenner, and Q. Chen, Phys. Rev. B **48**, 16 690 (1993).
[19] R. Gajić, E. K. H. Salje, Z. V. Popović, and H. L. Dewing, J. Phys.: Condens. Matter **4**, 9643 (1992).